IEEE Access
Multidisciplinary | Rapid Review | Open Access Journal

Received January 16, 2021, accepted January 17, 2021, date of publication January 22, 2021, date of current version February 1, 2021.

Digital Object Identifier 10.1109/ACCESS.2021.3053587

Current Sensor-Less Virtual Synchronous Generator Model Predictive Control Based on Sliding Mode Observer

YANYAN LI, WEITAO LI, LEILEI GUO, NAN JIN, (Member, IEEE), AND FALONG LU
College of Electrical and Information Engineering, Zhengzhou University of Light Industry, Zhengzhou 450002, China

Corresponding author: Leilei Guo (2006guoleilei@163.com)

This work was supported in part by the National Natural Science Foundation of China under Grant 51707176, in part by the Youth Talent Support Project of Henan Province under Grant 2019HYTP021, and in part by the Key Research, Development and Promotion Special Project (Science and Technology) of Henan Province under Grant 202102210103, Grant 202102210304, and Grant 212102210021.

ABSTRACT In recent years, virtual synchronous generator (VSG) control algorithm has been widely studied in distributed grid-connected power inverters to deal with active and reactive power adjustment by simulating the operation principle of the actual synchronous generator. Nevertheless, once the current sensor fails, the grid-connected power inverter will lose its stability. To enhance the fault-tolerant operation ability of the grid-connected power inverter, a new inverter side current sensor-less model predictive control method based on sliding mode observer (SMO) is proposed. The stability of the SMO is analyzed by using the Lyapunov stability criterion. The gains of the SMO are then designed by analyzing their influences on the current and voltage observation based on the closed-loop transfer functions. Besides, to show the influences of the capacitance changes on the current observation, a detailed parameter sensitivity analysis is also carried out. Then, by using the estimated inductance current from the SMO, a current sensor-less model predictive control method is finally proposed. The main novelty of the proposed method is that both the output voltage of the inverter and the inverter side inductance are not required in the proposed SMO. So, the accuracy of current sensor-less control is improved. To verify the effectiveness of the proposed method, detailed experimental studies are carried out based on a Typhoon and PE-Expert 4 based experimental platform.

INDEX TERMS Model predictive control, sensor-less control, sliding mode observer, VSG.

NOMENCLATURE

ω	Mechanical angular velocity
ω_0	Grid frequency
P_{ref}	Reference active power
P_e	Electromagnetic power
D_{eq}	Equivalent damping
J	Moment of inertia
$\boldsymbol{u}_{abc}$	Capacitor voltage
$\boldsymbol{i}_{\text{abc}}$	Grid-side current
θ	Reference voltage phase
ΔP	Adjusting active power
E	Output voltage
E_Q	Reactive power command
$\text{G}_i(s)$	Transfer function between the observed current and the sliding mode surface
n	Voltage droop coefficient
$\boldsymbol{V}_n$	The voltage vector
$\boldsymbol{V}_{\alpha\beta}$	The voltage on the inverter side
C	Filter capacitor
R	Parasitic resistance
Lg	Grid side inductance
Rg	Grid side resistance
$G(s)$	Transfer function between the observed current and the actual current
m	Frequency droop coefficient
V_{dc}	DC voltage
ξ	Quality factor
$\tilde{\boldsymbol{i}}_{f\alpha\beta}$	Current observation errors
$\tilde{\boldsymbol{u}}_{\alpha\beta}$	Voltage observation errors
$u_{\alpha ref}$	Reference power on $\alpha\beta$ axis
$u_{\beta ref}$	Reference power on $\alpha\beta$ axis
$G_{v1}(s)$	Transfer function between the sliding mode surface and the observed capacitor voltage

The associate editor coordinating the review of this manuscript and approving it for publication was Jinquan Xu.

e	The peak voltage of the grid
K_1	Gain of the SMO
K_2	Gain of the SMO
Q	Reactive power
$\boldsymbol{u}_{\alpha\beta}$	Capacitor voltage on the $\alpha\beta$ axis
F_1	Gain of the observer
F_2	Gain of the observer
$\boldsymbol{i}_{c\alpha\beta}$	Current of the capacitor
C_0	Capacitance parameter error
Q_{ref}	Reference reactive power
$\boldsymbol{i}_{f\alpha\beta}$	Output current of the inverter
L	Filter inductance
$\boldsymbol{i}_{\alpha\beta}$	Grid-side current on the $\alpha\beta$ axis
T	Sampling period

I. INTRODUCTION

When the conventional power electronic conversion interface is connected to the grid, the power system is easily affected by the power fluctuations and faults due to the lack of inertia and damping [1]. By using the virtual synchronous generator (VSG) scheme, the conventional grid-connected inverter can be controlled to simulate a traditional synchronous generator (SG), especially to simulate the inertia and damping [2]. By using the active power to regulate the frequency, and using the reactive power to adjust the voltage, VSG can work like a traditional SG [3]. Because of the use of VSG technologies, the power system that contains more and more renewable energy sources can operate with more security and stability.

Rencently, many relevant studies on VSG technologies have been published [4]–[10]. Typically, there are two types of VSG control technologies. In the first type, an outer power loop is used to regulate the frequency and the voltage [4]. At the same time, the inertia and damping are also simulated. Then, a modulation voltage is generated, which is fed into the pulse-width modulation block to control the inverter [2]–[6]. In the other type, there are often three control loops [7], including an outer power loop, which is used to adjust the frequency and the voltage, a middle voltage control loop, which is used to control the voltage of the filter capacitor, and an inner current loop, which takes the output current of the middle voltage control loop as the reference to control the output current of the inverter. Finally, a modulation voltage is generated by the inner current loop, which is fed into the pulse-widthmodulation block to control the inverter [8]–[10].

Although the above control methods have been widely studied, the design and debug of these methods are quite difficult because of the use of many proportional integral (PI) controllers.

In recent years, a new type of control method, which is named model predictive control (MPC), is receiving more and more attention because of its many advantages, such as easy to understand and extend, flexible to control different targets simultaneously, simple to implement with improved dynamic control performance, etc [11]–[16]. Reviews about MPC strategies are carried out by J. Rodriguez and R. Kennel in [11], [12], which show its wide application prospect.

T. Geyer studied multistep MPC in [13], which is very suitable for high-power converters and machine drives as its switching frequency can be reduced to several hundred hertz. Y. Zhang researched model predictive direct power control method for grid-connected inverters in [14], which is an alternative method to replace the conventional table-based direct power control to further improve the control performance. MPC strategies have also been studied in the back-to-back wind power system, such as [15]. The design of weighting factors, which are required to control several different targets simultaneously, are also studied in many papers, such as [16]. Other papers, such as [17]–[19], have also studied and verified the effectiveness of MPC strategies. All the results illustrated in [11]–[19] show the effectiveness and superiority of MPC in the region of power electronics and power drives. So, MPC has also been studied to control the VSG very recently in [20]–[22] by several researchers.

Compared with the conventional PI controller-based VSG control methods, MPC displayed its superiority in [20]–[22] for the control of VSG, such as easier to design and debug without the requirement to design PI controllers, faster dynamic process because of its direct voltage vector selection characteristic, and so on. So, in this paper, MPC based VSG control is further studied.

Although MPC methods are studied in [20]–[22] for VSG, it is necessary to detect the capacitor voltage, the inductor current, the grid voltage and current to accurately implement this typical VSG-MPC solution, which makes the system bulkily and increases hardware costs. Besides, physical sensors are prone to damage or make some measurement errors. Therefore, sensor-less control has been widely used for voltage source converter (VSC) to collect voltage and current signals [23]–[32], including L-filtered VSC [24], [25], LC-filtered VSC [26]–[29], and LCL-filtered VSC [30]–[33]. Among those sensor-less methods for VSCs, some papers use the output current of the inverter to observe the capacitor voltage and the grid current [23]. Other papers use the grid current and voltage to observe the capacitor voltage and the output current of the inverter [30]. In [28], a capacitance current sensor-less control method is designed for an LC-filtered VSC. In [31], an observer for inductor current estimation is developed based on the sampled capacitor voltage and grid current. Both the inverter side inductance and the filter capacitance are required in this observer, making it very sensitive to parameter changes. Moreover, as the output voltage of the inverter is also required, which is often affected by the dead zones and voltage drops on the power switches, the current observation precision may be further reduced.

In conclusion, many parameters, including the grid side inductance, the inverter side inductance, and the filter capacitance, are required in the above methods [23]–[33], which makes the observers very sensitive to parameter changes, reducing its observation accuracy.

This paper proposes an improved inverter side current sensor-less MPC method for VSG based a novel sliding mode observer (SMO), which observes the inverter side current using the sampled capacitor voltage and grid current. The novelty of this method is that only the information of the filter capacitance is required. So, compared to [31], the robustness of the proposed method against the inverter side inductance change is improved significantly. Moreover, the output voltage of the VSG is also not required in the proposed observer. So, the deadzone as well as the voltage drops on the power switches, which will influence the output voltage of the VSG, also has no effect on the proposed inverter side current observer. So, the current estimation accuracy can be further improved. That are the main contributions of this paper.

In this paper, the design method of the proposed SMO is studied in detail by using the Lyapunov stability theorem. Moreover, the selection method of the sliding mode gains is also studied by analyzing the closed-loop transfer function [33]. As the focus of this paper is fault-tolerant control (FTC) after sensor fails, detailed fault detection methods, which have been studied in [34]–[37], are not studied here.

II. VSG PRINCIPLE

A. BASIC VSG PRINCIPLE

The typical grid-connected inverter topology is shown in Fig. 1. As shown in Fig. 1, the proposed VSG control strategy is similar to the operating mechanism of a SG. The power conversion interface of inverter is controlled to emulate the inertial response and the damping power of a traditional SG [5].

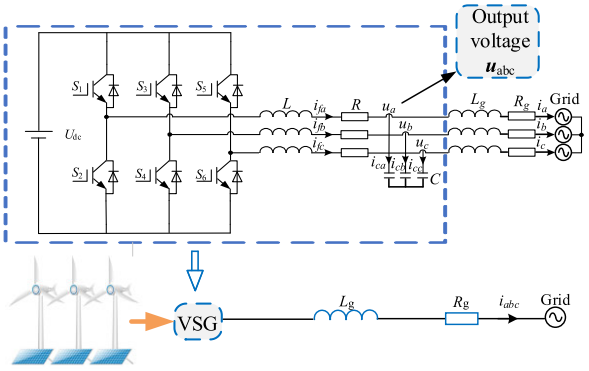

FIGURE 1. The topology of VSG.

According to Newton's second law, and assuming a virtual inertia constant J for the VSG unit, the swing equation of the VSG can be written as

$$P_{\text{ref}} - P_{\text{e}} - D_{\text{eq}}(\omega - \omega_0) = J\omega\frac{\text{d}\omega}{\text{d}t} \approx J\omega_0\frac{\text{d}\omega}{\text{d}t} \tag{1}$$

where ω represents the mechanical angular frequency, J is the moment of inertia of the VSG, ω_0 is the grid synchronous angular frequency, P_{ref} and P_{e} are the reference and the actual electromagnetic power of the VSG, respectively, and $D_{\text{eq}} = 1/m$ is the equivalent damping.

The active power P_{e} of the VSG is calculated from the capacitor voltage $\boldsymbol{u}_{\text{abc}}$ and the grid-side current $\boldsymbol{i}_{\text{abc}}$. To extract the fundamental active and reactive power, delayed-signal cancellation with multiple notch filters are used for harmonic elimination [8].

Thus, the active power P_e and reactive power Q calculation principles in the synchronous $\alpha\beta$ reference frame are formulated as

$$P_e = \frac{s^2 + \omega_0^2}{s^2 + 2\xi\omega_0 + \omega_0^2}1.5(u_\alpha i_\alpha + u_\beta i_\beta) \tag{2}$$

$$Q = \frac{s^2 + \omega_0^2}{s^2 + 2\xi\omega_0 + \omega_0^2}1.5(u_\beta i_\alpha - u_\alpha i_\beta) \tag{3}$$

where u_α and u_β are the components of the capacitor voltage $\boldsymbol{u}_{abc}$ on the $\alpha\beta$ coordinate system; i_α and i_β are the components of the grid-side current $\boldsymbol{i}_{abc}$ on the $\alpha\beta$ coordinate system; ω_0 represents the system fundamental frequency (it is set to $\omega_0 = 314$ rad/s in this paper), and ξ is the quality factor for the notch filters (it is set to $\xi = 0.5$ in this paper).

B. POWER REGULATION

The block diagram of Fig. 2 shows the frequency modulation approach and the voltage regulation method for the VSG algorithm, which has been explained in [8] in detail.

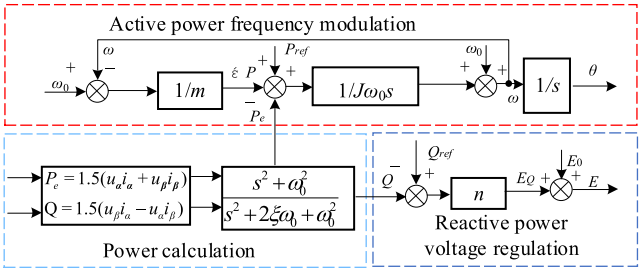

FIGURE 2. Block diagram of the VSG control system.

The swing equation of the VSG shown in (1) is illustrated as the active power frequency modulation block shown in Fig. 2. Here, ω_0 is the reference angular frequency. When the mechanical angular frequency ω of the VSG is smaller than the ω_0, dω/dt will be larger than zero when P_{e} is converged to P_{ref}. Thus, ω will be increased to ω_0. On the contrary, ω will be decreased to ω_0 if ω is larger than the ω_0. So, by using the active power frequency modulation control method shown in Fig.2, the mechanical angular frequency of the VSG will converge to the reference angular frequency finally. Thus, the system can operate steadily. Then, the reference voltage phase θ is obtained through integration.

The voltage droop block determines the output voltage E of the VSG, which is used to generate the reactive power command E_Q by calculating the difference between the reactive power Q and the reference reactive power Q_{ref}, and n is the reactive power droop coefficient. The voltage, frequency, active and reactive power of the inverter are controlled by the above two modules, and only parameters m, n and J are required.

Conventionally, by using the reference voltage generated by the above outer power loop, a middle voltage control loop and an inner current loop are often designed to further control the output voltage of the VSG [7]–[10]. However, many PI controllers are required, which makes the system difficult to design and debug.

The dynamic performance is also deteriorated because of the series control structure. To improve the control performance, an improved MPC based VSG control method is studied in this paper based the previous studies in [20]–[22].

III. PROPOSED CURRENT SENSOR-LESS PRINCIPLE

The MPC algorithm often predicts the state of the system in the next cycle using the current and all the available voltage vectors of the VSG at the present instant. Then, by comparison, an optimal control voltage vector is finally selected to control the VSG. Considering that the inverter has eight different switching states, eight voltage vectors $\boldsymbol{V}_0$, $\boldsymbol{V}_1$, $\boldsymbol{V}_2$, $\boldsymbol{V}_3$, $\boldsymbol{V}_4$, $\boldsymbol{V}_5$, $\boldsymbol{V}_6$, $\boldsymbol{V}_7$ can be generated correspondingly, as shown in Fig. 3.

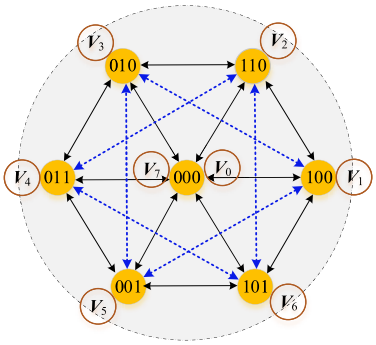

FIGURE 3. Voltage vectors.

A. CURRENT SENSOR-LESS VSG-MPC PRINCIPLE

The mathematical model of the LC-filtered VSG shown in Fig. 1 can be expressed as

$$\begin{cases} L\dfrac{\mathrm{d}\boldsymbol{i}_{f\alpha\beta}}{\mathrm{d}t} = \boldsymbol{V}_{\alpha\beta} - R\boldsymbol{i}_{f\alpha\beta} - \boldsymbol{u}_{\alpha\beta} \\ C\dfrac{\mathrm{d}\boldsymbol{u}_{\alpha\beta}}{\mathrm{d}t} = \boldsymbol{i}_{c\alpha\beta} = \boldsymbol{i}_{f\alpha\beta} - \boldsymbol{i}_{\alpha\beta} \end{cases} \tag{4}$$

where $\boldsymbol{V}_{\alpha\beta}$ is the voltage on the inverter side, $\boldsymbol{i}_{\alpha\beta}$ is the current on the grid side, $\boldsymbol{i}_{f\alpha\beta}$ is the output current of the inverter, L is inductor of the inverter side, C is capacitor of the LC filter, R is the parasitic resistance on the inverter side, $\boldsymbol{i}_{c\alpha\beta}$ is the current of the capacitor, $\boldsymbol{u}_{\alpha\beta}$ is the capacitor voltage.

To predict the capacitor voltage, the discretized model of VSG shown in (4) is derived as

$$\begin{cases} \dfrac{L}{T}\left[\boldsymbol{i}_{f\alpha\beta}\,(k+1) - \boldsymbol{i}_{f\alpha\beta}\,(k)\right] = \boldsymbol{V}\,(k) \\ -R\boldsymbol{i}_{f\alpha\beta}\,(k) - \boldsymbol{u}_{\alpha\beta}\,(k) \\ \dfrac{C}{T}\left[\boldsymbol{u}_{\alpha\beta}\,(k+1) - \boldsymbol{u}_{\alpha\beta}\,(k)\right] = \boldsymbol{i}_{c\alpha\beta}\,(k) = \boldsymbol{i}_{f\alpha\beta}\,(k+1) \\ -\boldsymbol{i}_{\alpha\beta}\,(k) \end{cases} \tag{5}$$

where T is control period.

From (5), it can be seen that the inductor current $\boldsymbol{i}_{f\alpha\beta}(k)$ and the capacitor voltage $\boldsymbol{u}_{\alpha\beta}(k)$ at k instant can be used to predict the inductor current $\boldsymbol{i}_{f\alpha\beta}(k+1)$ at $k+1$ instant. Then, by sampling the grid-connected current $\boldsymbol{i}_{\alpha\beta}(k)$, capacitor voltage $\boldsymbol{u}_{\alpha\beta}(k+1)$ can be further predicted. Finally, the optimal voltage vector value is selected to minimize the difference between the reference voltage generated by the outer power loop and the predicted voltage $\boldsymbol{u}_{\alpha\beta}(k+1)$.

Based on VSG-MPC, an improved current sensor-less voltage control is further proposed in this paper to improve the reliability of the VSG, especially under current sensor failure condition.

The proposed scheme contains three parts: a) an inverter side current observer, which is used to estimate the current and remove the current sensors, b) an improved MPC using the estimated current, which can be used to ensure the steady operation of the VSG under current sensor failure condition, c) an outer power loop, which is used to simulate an actual SG. The whole control block diagram is shown in Fig. 4.

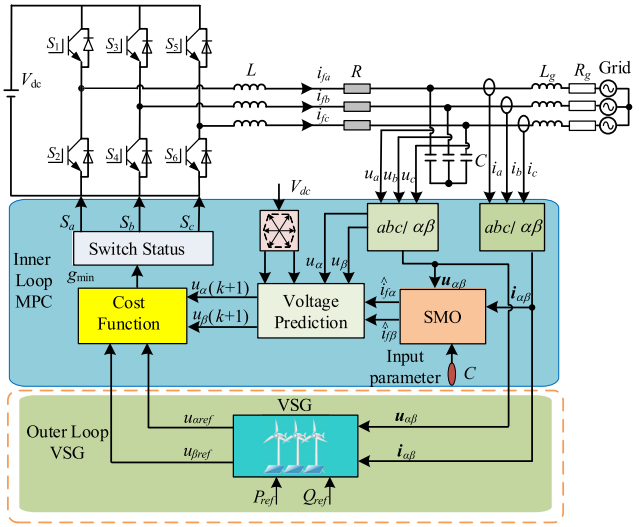

FIGURE 4. Model predictive control structure based on the virtual synchronous generator without the inductor current sensor.

B. INDUCTOR CURRENT OBSERVER DESIGN

The proposed observer in paper [31] is designed as

$$\begin{cases} \dfrac{\mathrm{d}\hat{\boldsymbol{i}}_{f\alpha\beta}}{\mathrm{d}t} = \dfrac{1}{L}(\boldsymbol{V}_{\alpha\beta} - \hat{\boldsymbol{u}}_{\alpha\beta}) + F_1(\boldsymbol{u}_{\alpha\beta} - \hat{\boldsymbol{u}}_{\alpha\beta}) \\ \dfrac{\mathrm{d}\hat{\boldsymbol{u}}_{\alpha\beta}}{\mathrm{d}t} = \dfrac{1}{C}\boldsymbol{i}_{f\alpha\beta} + F_2(\boldsymbol{u}_{\alpha\beta} - \hat{\boldsymbol{u}}_{\alpha\beta}) \end{cases} \tag{6}$$

where $\wedge$ represents the estimated value symbol, $\boldsymbol{V}_{\alpha\beta}$ is the output voltage of the inverter, F_1 and F_2 are the gains of the observer.

From (6), it can be seen that both the inverter side inductance and the filter capacitance are required in this observer, making it very sensitive to parameter changes. Moreover, as the output voltage of the inverter is also required, which is often affected by the dead zones and voltage drops on

the power switches, the current observation precision may be further reduced.

In this paper, to enhance the parameter robustness of the inverter side current observer and improve the current observation precision, a new current observer is designed.

Here, it is assumed that the current meet the condition shown in (7) as the amplitude and frequency of the current are changed slowly during a control period.

$$\frac{\mathrm{d}\boldsymbol{i}_{f\alpha\beta}}{\mathrm{d}t} = j\omega_0 \boldsymbol{i}_{f\alpha\beta} \tag{7}$$

To enhance the fault-tolerant operation ability of the VSG and achieve a comparable performance without using the inductor current sensor, a new current sensor-less VSG-MPC scheme is proposed as follows based on (7).

It is pointed out in [25] that the gains of the state observer should be selected carefully to ensure its stability, which is time consuming. On the contrary, SMO is more easy to design with a simplified structure and a strong robustness to parameter variations [35]. So, in this paper, different to the state observer in (6), a new SMO is designed, as shown in (8).

$$\begin{cases} \dfrac{\mathrm{d}\hat{\boldsymbol{i}}_{f\alpha\beta}}{\mathrm{d}t} = j\omega_0 \hat{\boldsymbol{i}}_{f\alpha\beta} + K_1 \mathrm{sgn}(\boldsymbol{u}_{\alpha\beta} - \hat{\boldsymbol{u}}_{\alpha\beta}) \\ C\dfrac{\mathrm{d}\hat{\boldsymbol{u}}_{\alpha\beta}}{\mathrm{d}t} = \hat{\boldsymbol{i}}_{f\alpha\beta} - \boldsymbol{i}_{\alpha\beta} + K_2 \mathrm{sgn}(\boldsymbol{u}_{\alpha\beta} - \hat{\boldsymbol{u}}_{\alpha\beta}) \end{cases} \tag{8}$$

where sgn $(\cdot)$ is the sign function, K_1 is the gain of the current SMO, K_2 is the gain of the capacitance-voltage SMO.

Based on (4), (7) and (8), the current and voltage observation errors can be obtained, as shown in (9).

$$\begin{cases} \dfrac{\mathrm{d}\bar{\boldsymbol{i}}_{f\alpha\beta}}{\mathrm{d}t} = j\omega_0 \bar{\boldsymbol{i}}_{f\alpha\beta} - K_1 \mathrm{sgn}(\bar{\boldsymbol{u}}_{\alpha\beta}) \\ C\dfrac{\mathrm{d}\bar{\boldsymbol{u}}_{\alpha\beta}}{\mathrm{d}t} = \bar{\boldsymbol{i}}_{f\alpha\beta} - K_2 \mathrm{sgn}(\bar{\boldsymbol{u}}_{\alpha\beta}) \end{cases} \tag{9}$$

where $\bar{\boldsymbol{i}}_{f\alpha\beta} = \boldsymbol{i}_{f\alpha\beta} - \hat{\boldsymbol{i}}_{f\alpha\beta}$, $\hat{\boldsymbol{u}}_{\alpha\beta} = \boldsymbol{u}_{\alpha\beta} - \hat{\boldsymbol{u}}_{\alpha\beta}$

In order to evaluate the stability of the designed SMO, the following Lyapunov function can be defined.

$$Y_1 = (\left|\bar{u}_\alpha^2\right| + \left|\bar{u}_\beta^2\right|)/2 \tag{10}$$

According to (10), it can be deduced that

$$\frac{dY_1}{dt} = \frac{\bar{i}_{f\alpha}\bar{u}_\alpha + \bar{i}_{f\beta}\bar{u}_\beta}{C} - \frac{K_2}{C}(|\bar{u}_\alpha| + \left|\bar{u}_\beta\right|) \tag{11}$$

According to the Lyapunov stability principle, to ensure the stability, $\mathrm{d}Y_1/\mathrm{d}t < 0$ should hold. Thus, it is deduced that the sliding mode gain must meet

$$K_2 > \max(\left|\bar{i}_{f\alpha}\right|, \left|\bar{i}_{f\beta}\right|) \tag{12}$$

The primary design method for the sliding mode gain K_2 is given by (12). Moreover, the detailed analysis of the sliding mode gains is given as follows.

Assuming that the capacitor voltage converges, the voltage SMO enters the sliding mode dynamics. So, $\bar{u}_\alpha = 0$ and $\bar{u}_\beta = 0$. Then, it can be known from the theory of sliding mode equivalent control that

$$\begin{cases} \bar{i}_{f\alpha} = K_2 \ \mathrm{sgn}(\bar{u}_\alpha) \\ \bar{i}_{f\beta} = K_2 0(\bar{u}_\beta) \end{cases} \tag{13}$$

The current observation errors on the $\alpha\beta$ coordinate system can be obtained from (9), which are shown in (14)

$$\begin{cases} \dfrac{\mathrm{d}\bar{i}_{f\alpha}}{\mathrm{d}t} = -\omega_0 \bar{i}_{f\beta} - \dfrac{K_1}{K_2}\bar{i}_{f\alpha} \\ \dfrac{\mathrm{d}\bar{i}_{f\beta}}{\mathrm{d}t} = \omega_0 \bar{i}_{f\alpha} - \dfrac{K_1}{K_2}\bar{i}_{f\beta} \end{cases} \tag{14}$$

Similarly, another Lyapunov function to evaluate the stability of the designed SMO for the inverter side current can be defined as

$$Y_2 = (\left|\bar{i}_{f\alpha}^2\right| + \left|\bar{i}_{f\beta}^2\right|)/2 \tag{15}$$

Then, it can be deduced that

$$\frac{\mathrm{d}Y_2}{\mathrm{d}t} = -\frac{K_1}{K_2}(\left|\bar{i}_{f\alpha}^2\right| + \left|\bar{i}_{f\beta}^2\right|) \tag{16}$$

If the SMO is stable, $\mathrm{d}Y_2/\mathrm{d}t < 0$ should hold. That is, the sliding mode gain K_1 needs to meet

$$K_1 > 0 \tag{17}$$

The basic sliding mode gain selection methods are shown in (12) and (17). To further study the influences of the sliding mode gains K_1 and K_2 on the observation of the current, another research is carried out in the following by analyzing the bode diagram of the closed-loop transfer function [33].

After the capacitor voltage converges, according to (7) and (8), the following transfer function can be obtained

$$G(s) = \frac{\hat{\boldsymbol{i}}_{f\alpha\beta}(s)}{\boldsymbol{i}_{f\alpha\beta}(s)} = \frac{K_1/K_2}{(s - j\omega_0 + K_1/K_2)} \tag{18}$$

Then, it can be seen that when $s = j\omega_0$, $\hat{\boldsymbol{i}}_{f\alpha\beta} = \boldsymbol{i}_{f\alpha\beta}$ is obtained, meaning that the proposed observer can estimate the current accurately. Meanwhile, from (18) it is easy to known that K_1 and K_2 determine the dynamic and steady state control performance of the SMO.

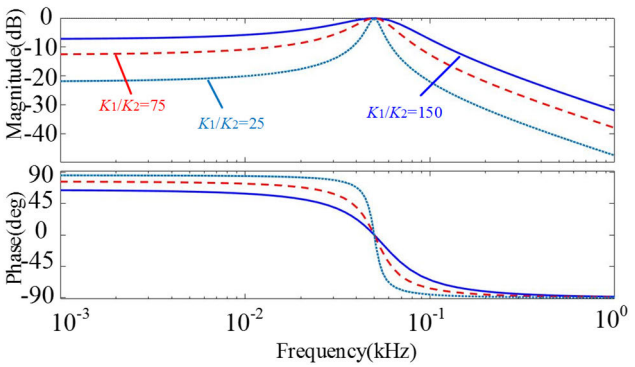

FIGURE 5. Bode diagrams of the transfer function $G(s)$.

The Bode diagram of the transfer function $G(s)$ in (18) is shown in Fig. 5 with different K_1/K_2. With the increasement

of the sliding mode gain K_1/K_2, the bandwidth of $G(s)$ increases, which means a faster dynamic response speed can be obtained. However, sliding mode noise will be amplified when K_1/K_2 increases, which means that the sliding mode observer's steady-state performance deteriorates. Therefore, appropriate sliding mode gains should be selected to make a compromise.

In this paper, since the sliding mode gain K_2 accounts for a small proportion of the observed voltage (8), unreasonable K_2 will inevitably affect the observed inductor current. According to formula (12), K_2 should be larger than 0. Therefore, K_2 here is set as 2. Then, K_1 is further selected.

To further design the SMO, the transfer function of the sliding mode surface to the estimated current and the sliding mode surface to the estimated voltage are also analyzed.

According to (8), the transfer function $G_i(s)$ between the observed current and the sliding mode surface is

$$G_i(s) = \frac{\hat{\boldsymbol{i}}_{f\alpha\beta}(s)}{\boldsymbol{s}_{\alpha\beta}(s)} = \frac{K_1}{(s - j\omega_0)} \tag{19}$$

where $\boldsymbol{s}_{\alpha\beta} = \mathrm{sgn}(\bar{\boldsymbol{u}}_{\alpha\beta})$.

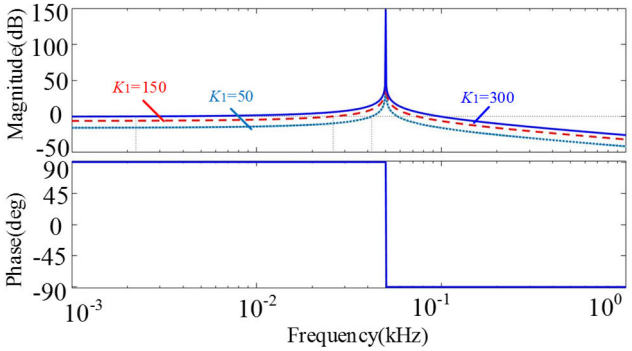

FIGURE 6. Bode diagrams of the transfer function $G_i(s)$.

The Bode diagram of the transfer function $G_i(s)$ in (19) is shown in Fig. 6 when K_1 is changed. It can be seen from Fig. 6 that with the increment of the sliding mode gain K_1, the bandwith of the transfer function $G_i(s)$ is also increased, meaning the dynamic convergence speed of the SMO is enhanced. However, the sliding mode noise will also be magnified. Thus, K_1 is also should be selected to make a compromise.

The transfer function $G_{v1}(s)$ between the sliding mode surface and the observed capacitor voltage can be obtained from (8) and (19), which is shown in (20).

$$\boldsymbol{G}_{v1}(s) = \frac{[K_1 + K_2(s - j\omega_0)]\boldsymbol{s}_{\alpha\beta} - \boldsymbol{i}_{\alpha\beta}(s - j\omega_0)}{Cs(s - j\omega_0)} \tag{20}$$

Here, $\boldsymbol{i}_{\alpha\beta}$ is a disturbance. When it is ignored, (21) is obtained.

$$G_v(s) = \frac{\hat{\boldsymbol{u}}_{\alpha\beta}(s)}{\boldsymbol{s}_{\alpha\beta}(s)} = \frac{K_1 + K_2(s - j\omega_0)}{Cs(s - j\omega_0)} \tag{21}$$

According to (21), Bode diagrams can be plotted to analyze the influences of the sliding mode gain, as shown in Fig. 7.

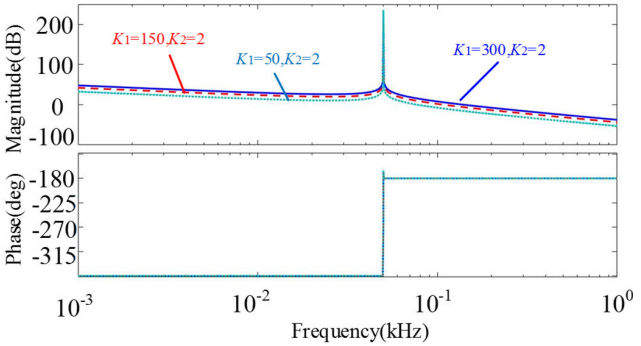

FIGURE 7. Bode diagrams of the transfer function $G_v(s)$.

It can be seen from Fig. 7 that the larger the K_1, the larger the bandwidth of $G_v(s)$. However, the sliding mode noise will also be magnified. As K_1 and K_2 should be selected by considering the dynamic and steady state control performance of the SMO simultaneously, K_1 is finally set as 150.

C. CAPACITANCE ERROR ANALYSIS

Considering that the filter capacitance is required in the proposed SMO, its influences are analyzed in the following. When the capacitance parameter C has an error C_0, the SMO in (8) can be reconstructed as

$$\begin{cases} \dfrac{\mathrm{d}\hat{\boldsymbol{i}}_{f\alpha\beta}}{\mathrm{d}t} = j\omega_0\hat{\boldsymbol{i}}_{f\alpha\beta} + K_1\mathrm{sgn}(\boldsymbol{u}_{\alpha\beta} - \hat{\boldsymbol{u}}_{\alpha\beta}) \\ (C + C_0)\dfrac{\mathrm{d}\hat{\boldsymbol{u}}_{\alpha\beta}}{\mathrm{d}t} = \hat{\boldsymbol{i}}_{f\alpha\beta} - \boldsymbol{i}_{\alpha\beta} + K_2\mathrm{sgn}(\boldsymbol{u}_{\alpha\beta} - \hat{\boldsymbol{u}}_{\alpha\beta}) \end{cases} \tag{22}$$

The current and voltage observation errors can be obtained from (8) and (22)

$$\begin{cases} \dfrac{\mathrm{d}\bar{i}_{f\alpha\beta}}{\mathrm{d}t} = j\omega_0\bar{i}_{f\alpha\beta} - K_1\mathrm{sgn}(\bar{u}_{\alpha\beta}) \\ C\dfrac{\mathrm{d}\bar{u}_{\alpha\beta}}{\mathrm{d}t} - C_0\dfrac{\mathrm{d}\hat{u}_{\alpha\beta}}{\mathrm{d}t} = \bar{i}_{f\alpha\beta} - K_2\mathrm{sgn}(\bar{u}_{\alpha\beta}) \end{cases} \tag{23}$$

When the observer converges, that is, the voltage converges, it can be obtained that

$$\frac{\mathrm{d}\bar{\boldsymbol{i}}_{f\alpha\beta}}{\mathrm{d}t} = j\omega_0\bar{\boldsymbol{i}}_{f\alpha\beta} - \frac{K_1}{K_2}(\bar{\boldsymbol{i}}_{f\alpha\beta} + C_0\frac{\mathrm{d}\hat{\boldsymbol{u}}_{\alpha\beta}}{\mathrm{d}t}) \tag{24}$$

Finally, the formula for the influence of the capacitance error on the observed current can be obtained

$$\hat{\boldsymbol{i}}_{f\alpha\beta} = \frac{C + C_0}{C}\boldsymbol{i}_{f\alpha\beta} - \frac{C_0}{C}\boldsymbol{i}_{\alpha\beta} \tag{25}$$

It can be seen from (25) that if $C_0 = 0$, $\hat{\boldsymbol{i}}_{f\alpha\beta} = \boldsymbol{i}_{f\alpha\beta}$, meaning that the current observation error is zero. Otherwise, once $C_0 \neq 0$, there will be an current estimation error. That's the drawback of the proposed method. Fortunately, the experimental results given in Section IV shows that the influences of the capacitance error on the voltage control are quite small.

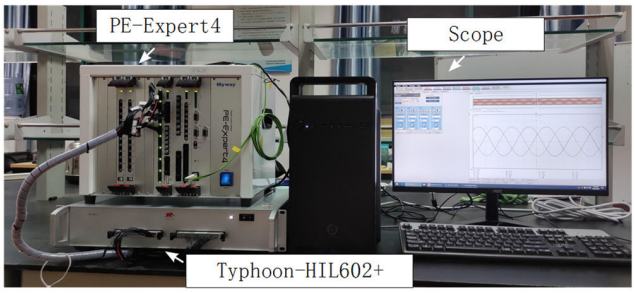

FIGURE 8. Experimental setup.

IV. HIL EXPERIMENT VALIDATION

To evaluate the performance of the proposed method and the accuracy of the estimated inverter side current, an experiment platform is designed as shown in Fig. 8, which includes a simulator of Typhoon602+ and a controller of PE-Expert4. All the control algorithms are executed in the PE-Expert4 processor board, which consists of DSP and FPGA control chips.

A. FAULT DETECTION RESULTS

In the first study, the fault-tolerant operation ability of the grid-connected power inverter is evaluated when the current sensor fails.

To compare the two control methods fairly, the VSG droop coefficient, virtual inertia, and low-pass filter cut-off frequency are the same for the conventional VSG-MPC method and proposed method. Table 1 summarizes the key parameters of the proposed scheme.

TABLE 1. The parameters of the proposed system.

Variable	Parameter	Value
V_{dc}	DC voltage	500V
e	The peak voltage of the grid	190V
L	Filter inductance	6.4mH
C	Filter capacitor	70μF
R	Parasitic resistance	0.1Ω
L_g	Grid side inductance	0.001H
T	Sampling period	25μs
R_g	Grid side resistance	2Ω
m	Frequency droop coefficient	0.0003
n	Voltage droop coefficient	0.05
j	Moment of inertia	0.00005
ω_0	Grid frequency	100π

Fig. 9(a) depicts the experimental results after the failure of the C-phase current sensor. It can be seen that the system loses its stability because of the fault of the current sensor. On the contrary, Fig. 9(b) shows the experimental results when using the estimated current to replace the faulty one. Then, the system returns to stable operation. That means the proposed method can be used as a flexible backup resource to ensure the system work continuously under current sensors fail conditions.

It should be pointed out that as the focus of this paper is fault-tolerant control (FTC) after sensor fails. Detailed fault detection methods, which have been studied in [34]–[37], are not studied here. In the fault detection experiment, the C-phase current i_{fc} is set to zero artificially to simulate the broken-line fault of the C-phase current sensor. Then, after a delay of 3.5ms, the estimated inverter side current is used to replace the fault one, i.e. The proposed current sensor-less VSG-MPC method is used. Then, the system returns to stable, as shown in Fig.9(b).

B. DYNAMIC EXPERIMENTAL RESULTS

In the second study, the power regulation performance of the VSG based the proposed inverter side current observer is evaluated under different operation conditions.

First, the performance when the actual power changes is tested. Here, the reference actual power is changed from 500W to 1500W. Fig. 10 shows the inertia change process of the actual power as well as the output current and voltage of the VSG when the conventional VSG-MPC and the proposed current sensor-less VSG-MPC are utilized, respectively.

As shown in Fig. 10(a) and Fig. 10(b), when P_{ref} is changed, the inverter side current $i_{f\beta}$, the capacitance voltage $u_{\beta,}$ and the reactive power Q fluctuated. However, both of the two methods have similar dynamic control performance. Moreover, in the steady-state, as indicated by the zoom-in voltage and current shown in Fig. 10(c) and Fig. 10(d), compared with the conventional VSG-MPC method, although the inductor current ripple becomes a little larger than the conventional method, the capacitance-voltage values of the proposed method also maintain an excellent tracking state. So, it is concluded that proposed method achieves a satisfactory dynamic and steady state control performance with reduced current sensors, which is comparable to the conventional VSG-MPC method. That shows the effectiveness of the proposed current sensor-less MPC method.

Besides, to further demonstrate the accuracy of the proposed method under reactive power regulation, another experimental study is carried out.

Fig. 11 shows the experimental results of the voltage, the current, and the power using the conventional VSG-MPC and the proposed VSG-MPC control method, respectively.

To show the process of reactive power regulation, the reference reactive power Q_{ref} is stepped up from 0Var to 200Var. From Fig. 11, it is obvious to see that compared with the conventional VSG-MPC method, the proposed current sensor-less control method can achieve a comparable power and voltage control performance with reduced hardware cost, which further verifies the effectiveness of the proposed current sensor-less MPC method.

In summary, the proposed method can operate with comparable steady and dynamic state control performance (a little

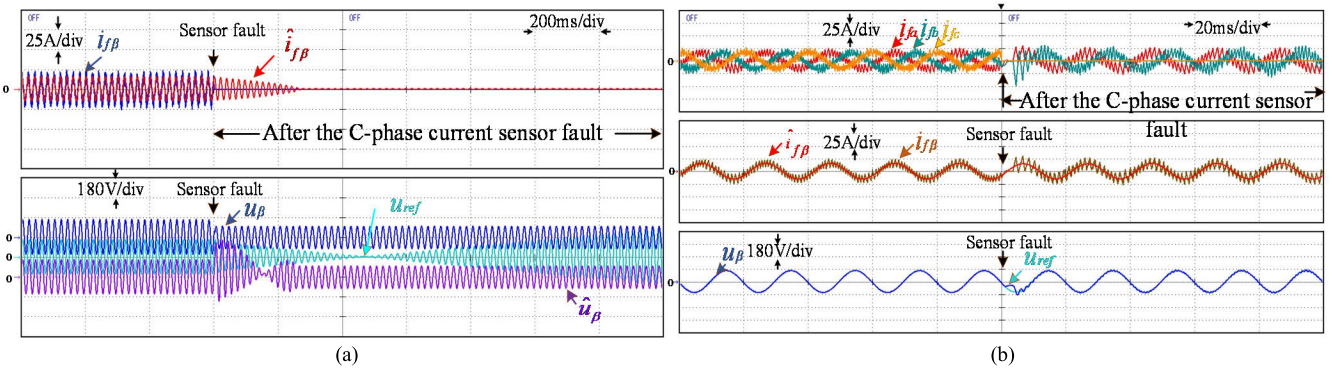

FIGURE 9. Sensor fault experimental results. (a) No treatment after failure. (b) Replace the current sensor with the estimated value after the fault.

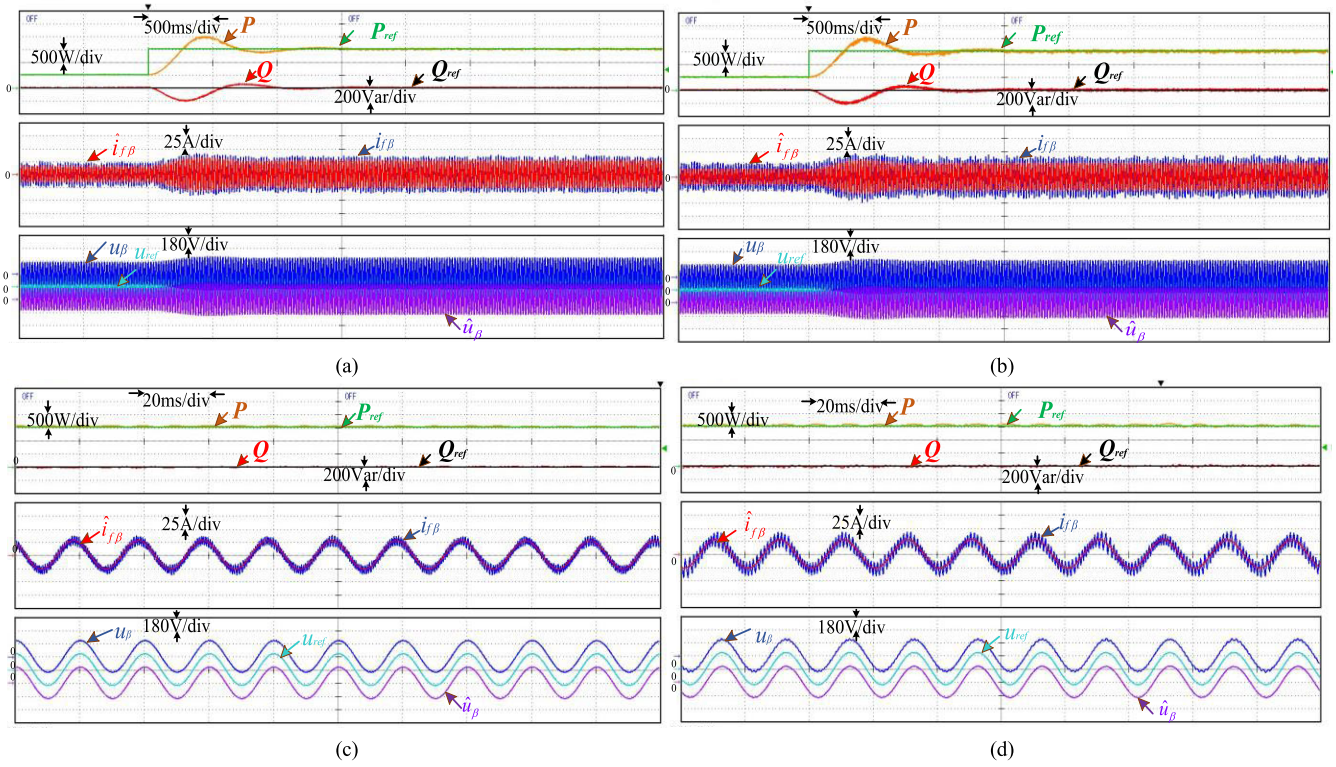

FIGURE 10. Experimental results when the reference P_{ref} increase from 500W to1500W. (a) VSG-MPC power control. (b) Current sensor-less VSG-MPC power control. (c) Enlargement of steady performance in FIGURE 10(a). (d) Enlargement of steady performance in FIGURE 10(b).

bit larger current ripple but acceptable) as the conventional VSG-MPC control. Moreover, the stronger current sensor substitutability to distributed grid-connected power inverters can be obtained by the proposed method.

C. PARAMETER MISMATCH EXPERIMENTAL

In the third study, as the proposed current observer requires the information of the capacitor parameter its influences are further tested here. The results are shown in Fig. 12.

As shown in Fig. 12(a), when the capacitance parameter used in the observer becomes larger than the actual value, a current estimation error is generated and the observed current leads the actual one with an enlarged amplitude. On the contrary, when the capacitance becomes smaller, a current estimation error is also generated and the observed current lags the actual one with an reduced amplitude.

Fortunately, although the imprecise capacitor parameter will affect the current observation, its influences on the control of the capacitor voltage control are very small, as shown in the second figure in Fig. 12(a) and 12(b). Additionally, it is worth mentioning that although a deviation is generated in the estimated current when capacitance parameter becomes smaller, the steady state voltage control performance is still satisfactory after a short dynamic process, which indicates

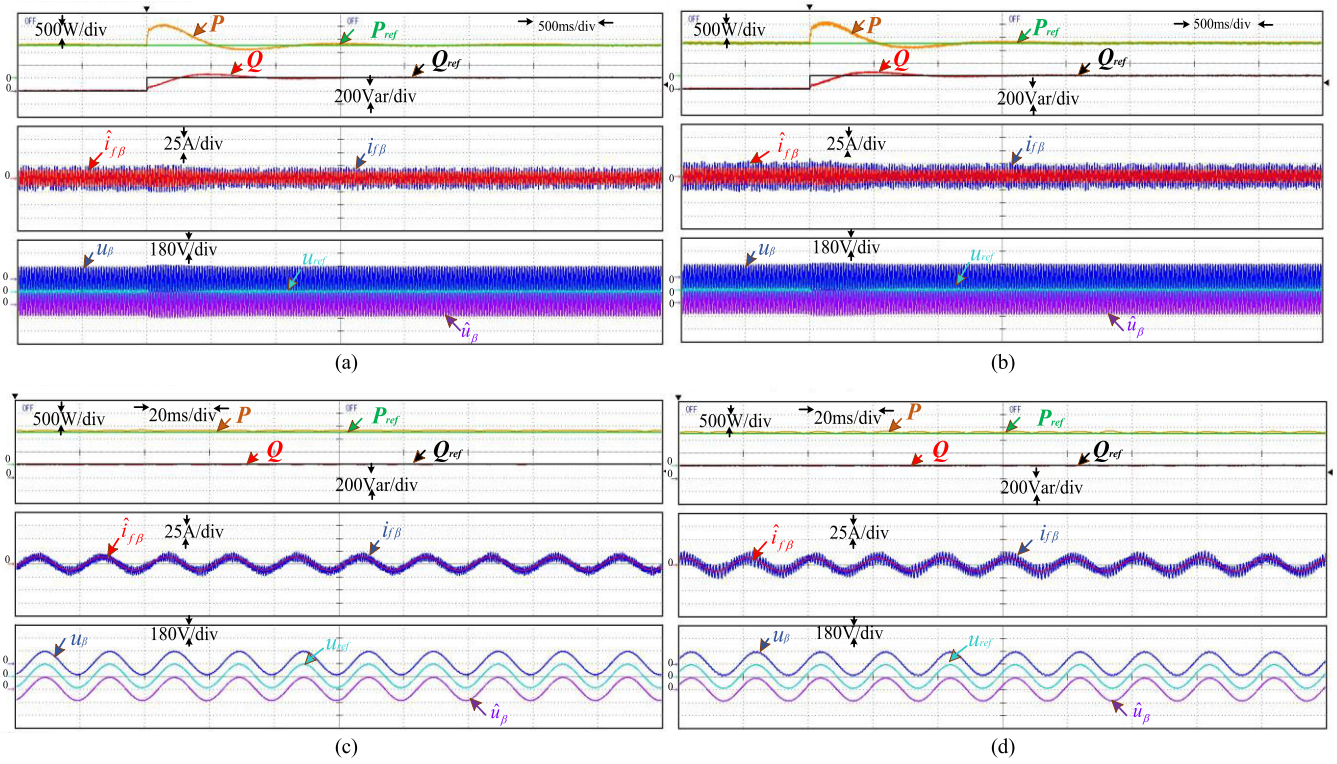

FIGURE 11. Experimental results when the reference Q_{ref} increase from 0Var to 200Var. (a) VSG-MPC power control. (b) Current sensor-less VSG-MPC power control. (c) Enlargement of steady performance in FIGURE11 (a). (d) Enlargement of steady performance in FIGURE11 (b).

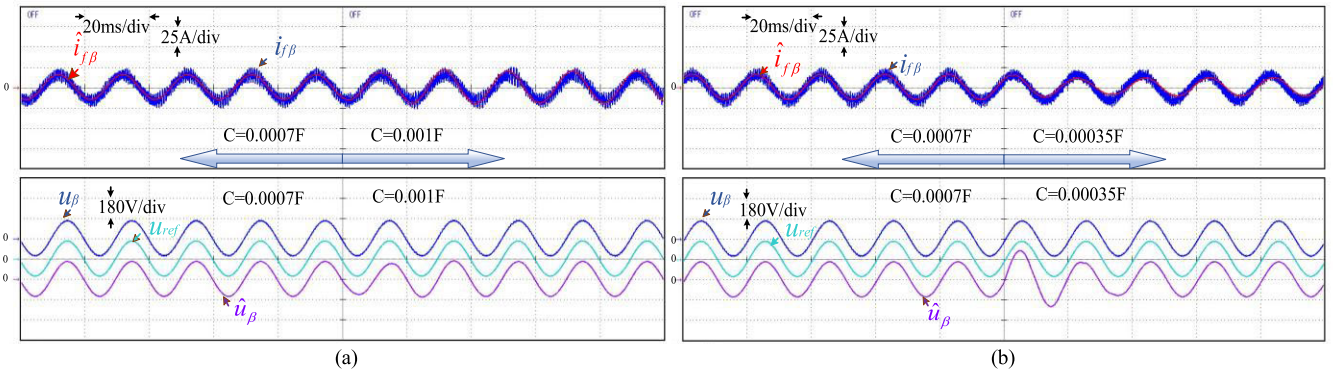

FIGURE 12. The capacitance parameter mismatch experimental results. (a) The capacitance parameter is increased to 0.001F. (b) The capacitance parameter is reduced to 0.00035F.

that the steady state voltage control performance of the proposed method does not suffer from the parameter mismatch so much.

D. COMPARISON WITH PI CONTROL

To further compare the proposed method with the conventional PI linear control based on VSG, another test is also carried out. Here, the second type VSG control method studied in [7]–[10] based on PI linear control is researched. To ensure a fair comparison, the switching frequency of the PI linear control is set as 4kHz, and the average switching frequency of the proposed MPC strategy is set as 4kHz, too. Here, only the voltage control loop is tested to compare the steady and dynamic control performance.

Fig. 13 shows the test results of the voltage response using the conventional PI linear control and the proposed MPC method respectively under a step change of the reference voltage.

As shown in Fig. 13, the voltage fluctuation and settling time of the conventional PI linear control method are larger than the proposed MPC. Although PI parameters can be adjusted to achieve a better control performance, it is very hard to balance the steady and dynamic state control performance as the two targets are inherent inhibitory. It is attractive

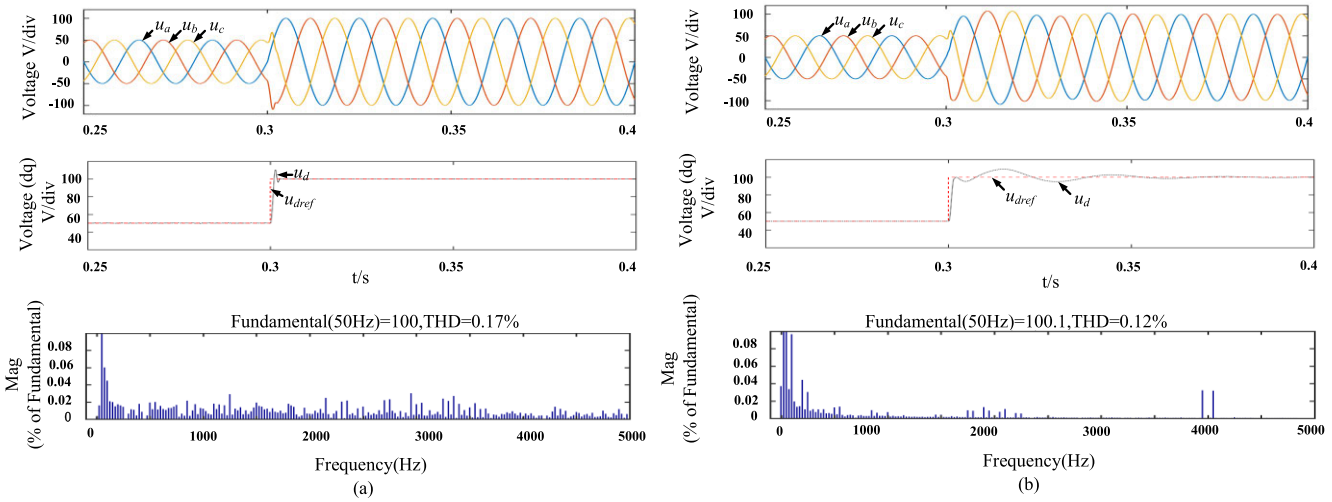

FIGURE 13. Test results of voltage dynamic response. (a) The proposed MPC method. (b) Conventional PI Linear control.

to see that the proposed MPC has a very fast voltage recovery capability, which shows its superiority obviously.

However, from the voltage spectrum it can be seen that the voltage THD of the conventional PI linear control method is smaller than that of the proposed MPC strategy. That is mainly because of the variable switching frequency characteristic of the proposed MPC strategy. Nevertheless, the voltage THD of the proposed MPC strategy is still comparable with the conventional PI linear control method.

So, it can be concluded that compared with the conventional PI linear control method, the proposed MPC strategy in this paper can achieve a very fast dynamic control performance with a comparable steady control performance. That's why MPC have been studied by many researchers in the field of power electronics and power drives in recent years [11]–[22].

V. DISCUSSION AND CONCLUSION

This paper proposes an inverter side current sensor-less control method for VSG, which ensures the stable operation after current sensor fails. Firstly, to estimate the inverter side current, a SMO is designed. Then, the gains of the proposed SMO are designed carefully based on the Lyapunov stability criterion and the closed-loop transfer function. Additionally, the influences of the capacitance mismatch on the proposed current observation method are also analyzed in detail, which shows that it has little effect on the voltage control. Finally, based on the presented current observation method, a current sensor-less VSG-MPC strategy is established. The hardware-in-the-loop experiment study verifies the effectiveness of the proposed method.

REFERENCES

[1] F. Gao and M. R. Iravani, "A control strategy for a distributed generation unit in grid-connected and autonomous modes of operation," *IEEE Trans. Power Del.*, vol. 23, no. 2, pp. 850–859, Apr. 2008.

[2] Q.-C. Zhong and G. Weiss, "Synchronverters: Inverters that mimic synchronous generators," *IEEE Trans. Ind. Electron.*, vol. 58, no. 4, pp. 1259–1267, Apr. 2011.

[3] Y. Chen, R. Hesse, D. Turschner, and H.-P. Beck, "Improving the grid power quality using virtual synchronous machines," in *Proc. Int. Conf. Power Eng., Energy Electr. Drives*, May 2011, pp. 1–6.

[4] G. Yao, Z. Lu, Y. Wang, M. Benbouzid, and L. Moreau, "A virtual synchronous generator based hierarchical control scheme of distributed generation systems," *Energies*, vol. 10, no. 12, p. 2049, Dec. 2017.

[5] T. El Tawil, G. Yao, J. F. Charpentier, and M. Benbouzid, "Design and analysis of a virtual synchronous generator control strategy in microgrid application for stand-alone sites," *IET Gener., Transmiss. Distrib.*, vol. 13, no. 11, pp. 2154–2161, Jun. 2019.

[6] A. Belila, Y. Amirat, M. Benbouzid, E. M. Berkouk, and G. Yao, "Virtual synchronous generators for voltage synchronization of a hybrid PV-diesel power system," *Int. J. Electr. Power Energy Syst.*, vol. 117, May 2020, Art. no. 105677.

[7] Z. Qu, H. Yang, J. Han, C. Song, W. Li, and Y. Cai, "Effects analysis of excitation circuit on power control for VSG: A design-oriented study," *IET Renew. Power Gener.*, vol. 14, no. 5, pp. 803–810, Apr. 2020.

[8] H. Xu, X. Zhang, F. Liu, R. Shi, C. Yu, and R. Cao, "A reactive power sharing strategy of VSG based on virtual capacitor algorithm," *IEEE Trans. Ind. Electron.*, vol. 64, no. 9, pp. 7520–7531, Sep. 2017.

[9] R. Shi, X. Zhang, H. Xu, F. Liu, and W. Cao, "Research on the synchronization control strategy for microgrid inverter," in *Proc. Int. Power Electron. Appl. Conf. Expo.*, Shanghai, China, Nov. 2014, pp. 210–213.

[10] X. Meng, J. Liu, and Z. Liu, "A generalized droop control for grid-supporting inverter based on comparison between traditional droop control and virtual synchronous generator control," *IEEE Trans. Power Electron.*, vol. 34, no. 6, pp. 5416–5438, Jun. 2019.

[11] S. Vazquez, J. Rodriguez, M. Rivera, L. G. Franquelo, and M. Norambuena, "Model predictive control for power converters and drives: Advances and trends," *IEEE Trans. Ind. Electron.*, vol. 64, no. 2, pp. 935–947, Feb. 2017.

[12] P. Karamanakos, E. Liegmann, T. Geyer, and R. Kennel, "Model predictive control of power electronic systems: Methods, results, and challenges," *IEEE Open J. Ind. Appl.*, vol. 1, pp. 95–114, 2020.

[13] T. Geyer and D. E. Quevedo, "Performance of multistep finite control set model predictive control for power electronics," *IEEE Trans. Power Electron.*, vol. 30, no. 3, pp. 1633–1644, Mar. 2015.

[14] H. Yang, Y. Zhang, and J. Liu, "Frequency-adaptive virtual flux estimator-based predictive power control with suppression of DC voltage ripples under unbalanced network," *IEEE Trans. Ind. Electron.*, vol. 67, no. 10, pp. 8969–8979, Oct. 2020.

[15] Z. Zhang, C. M. Hackl, and R. Kennel, "Computationally efficient DMPC for three-level NPC back-to-back converters in wind turbine systems with PMSG," *IEEE Trans. Power Electron.*, vol. 32, no. 10, pp. 8018–8034, Oct. 2017.

[16] S. A. Davari, V. Nekoukar, C. Garcia, and J. Rodriguez, "Online weighting factor optimization by simplified simulated annealing for finite set predictive control," *IEEE Trans. Ind. Informat.*, vol. 17, no. 1, pp. 31–40, Jan. 2021.
[17] L. Guo, N. Jin, C. Gan, L. Xu, and Q. Wang, "An improved model predictive control strategy to reduce common-mode voltage for two-level voltage source inverters considering dead-time effects," *IEEE Trans. Ind. Electron.*, vol. 66, no. 5, pp. 3561–3572, May 2019.
[18] N. Jin, S. Hu, C. Gan, and Z. Ling, "Finite states model predictive control for fault-tolerant operation of a three-phase bidirectional AC/DC converter under unbalanced grid voltages," *IEEE Trans. Ind. Electron.*, vol. 65, no. 1, pp. 819–829, Jan. 2018.
[19] L. Guo, N. Jin, C. Gan, and K. Luo, "Hybrid voltage vector preselection-based model predictive control for two-level voltage source inverters to reduce the common-mode voltage," *IEEE Trans. Ind. Electron.*, vol. 67, no. 6, pp. 4680–4691, Jun. 2020.
[20] C. Zheng, T. Dragicevic, and F. Blaabjerg, "Model predictive control based virtual inertia emulator for an islanded AC microgrid," *IEEE Trans. Ind. Electron.*, early access, Jul. 10, 2020, doi: 10.1109/TIE.2020.3007105.
[21] Y. Sun, Y. Zhao, Z. Dou, Y. Li, and L. Guo, "Model predictive virtual synchronous control of permanent magnet synchronous generator-based wind power system," *Energies*, vol. 13, no. 19, p. 5022, Sep. 2020.
[22] N. Jin, C. Pan, Y. Li, S. Hu, and J. Fang, "Model predictive control for virtual synchronous generator with improved vector selection and reconstructed current," *Energies*, vol. 13, no. 20, p. 5435, Oct. 2020.
[23] Z. Wang, S. Li, J. Yang, and Q. Li, "Current sensor-less sliding mode control for direct current alternating current inverter with load variations via a USDO approach," *IET Power Electron.*, vol. 11, no. 8, pp. 1389–1398, Jul. 2018.
[24] S. G. Jorge, J. A. Solsona, and C. A. Busada, "Control scheme for a single-phase grid-tied voltage source converter with reduced number of sensors," *IEEE Trans. Power Electron.*, vol. 29, no. 7, pp. 3758–3765, Jul. 2014.
[25] L. Guo, N. Jin, Y. Li, and K. Luo, "A model predictive control method for grid-connected power converters without AC voltage sensors," *IEEE Trans. Ind. Electron.*, vol. 68, no. 2, pp. 1299–1310, Feb. 2021.
[26] H. Bai, X. Wang, and F. Blaabjerg, "A grid-voltage-sensorless resistive-active power filter with series LC-filter," *IEEE Trans. Power Electron.*, vol. 33, no. 5, pp. 4429–4440, May 2018.
[27] S. Vazquez, A. Marquez, J. I. Leon, L. G. Franquelo, and T. Geyer, "FCS-MPC and observer design for a VSI with output LC filter and sinusoidal output currents," in *Proc. 11th IEEE Int. Conf. Compat., Power Electron. Power Eng.*, Apr. 2017, pp. 677–682.
[28] C. Zheng, T. Dragicevic, and F. Blaabjerg, "Current-sensorless finite-set model predictive control for LC-filtered voltage source inverters," *IEEE Trans. Power Electron.*, vol. 35, no. 1, pp. 1086–1095, Jan. 2020.
[29] M. Su, B. Cheng, Y. Sun, Z. Tang, B. Guo, Y. Yang, F. Blaabjerg, and H. Wang, "Single-sensor control of LCL-filtered grid-connected inverters," *IEEE Access*, vol. 7, pp. 38481–38494, Mar. 2019.
[30] J. Zhao, W. Wu, Z. Shuai, A. Luo, H. S.-H. Chung, and F. Blaabjerg, "Robust control parameters design of PBC controller for LCL-filtered grid-tied inverter," *IEEE Trans. Power Electron.*, vol. 35, no. 8, pp. 8102–8115, Aug. 2020.
[31] Z. Zhang, A. W. Oluwafemi, M. Hosseinzadehtaher, and M. B. Shadmand, "Current observer based predictive decoupled power control grid-interactive inverter," in *Proc. IEEE Texas Power Energy Conf. (TPEC)*, College Station, TX, USA, Feb. 2020, pp. 1–6.
[32] R. A. Fantino, C. A. Busada, and J. A. Solsona, "Observer-based grid-voltage sensorless synchronization and control of a VSI-LCL tied to an unbalanced grid," *IEEE Trans. Ind. Electron.*, vol. 66, no. 7, pp. 4972–4981, Jul. 2019.
[33] H. Yang, Y. Zhang, and P. Huang, "Improved predictive current control of IM drives based on a sliding mode observer," in *Proc. IEEE Int. Symp. Predictive Control Electr. Drives Power Electron. (PRECEDE)*, Quanzhou, China, May 2019, pp. 1–6, doi: 10.1109/PRECEDE.2019.8753274.
[34] Y. Yu, Y. Zhao, B. Wang, X. Huang, and D. Xu, "Current sensor fault diagnosis and tolerant control for VSI-based induction motor drives," *IEEE Trans. Power Electron.*, vol. 33, no. 5, pp. 4238–4248, May 2018.
[35] G. Wang, X. Hao, N. Zhao, G. Zhang, and D. Xu, "Current sensor fault-tolerant control strategy for encoderless PMSM drives based on single sliding mode observer," *IEEE Trans. Transport. Electrific.*, vol. 6, no. 2, pp. 679–689, Jun. 2020.
[36] B. Tabbache, N. Rizoug, M. E. H. Benbouzid, and A. Kheloui, "A control reconfiguration strategy for post-sensor FTC in induction motor-based EVs," *IEEE Trans. Veh. Technol.*, vol. 62, no. 3, pp. 965–971, Mar. 2013, doi: 10.1109/TVT.2012.2232325.
[37] B. Tabbache, M. E. H. Benbouzid, A. Kheloui, and J.-M. Bourgeot, "Virtual-sensor-based maximum-likelihood voting approach for fault-tolerant control of electric vehicle powertrains," *IEEE Trans. Veh. Technol.*, vol. 62, no. 3, pp. 1075–1083, Mar. 2013, doi: 10.1109/TVT.2012.2230200.

YANYAN LI was born in Henan, China, in 1987. She received the Ph.D. degree in control science and engineering from the Tianjin Key Laboratory Of Intelligent Robotics, College of Artificial Intelligence, Nankai University, Tianjin, China, in 2017.

She is currently a Lecturer with the Zhengzhou University of Light Industry, Zhengzhou, China. Her current research interests include model predictive control for power converters, grid impedance identification, and tolerant control of power electronics systems.

WEITAO LI was born in Linzhou, China, in 1996. He received the B.S. degree in electrical engineering from the Zhongyuan University of Technology, Zhengzhou, China, in 2019. He is currently pursuing the master's degree with the Zhengzhou University of Light Industry. His research interests include mode predictive control for power converters.

LEILEI GUO was born in Henan, China, in 1987. He received the B.S. and Ph.D. degree in electrical engineering from the School of Electrical Engineering and Automation, Hefei University of Technology, Hefei, China, in 2010 and 2016, respectively.

He is currently a Lecturer with the Zhengzhou University of Light Industry. He was selected into the young talent promotion plan of Henan province, in 2018. He has published more than 30 technical articles in journals and conference proceedings. His current research interests include model predictive control of induction motors, permanent-magnet synchronous motors, and power converters.

NAN JIN (Member, IEEE) received the B.S. and M.S. degrees in electrical engineering from the Zhengzhou University of Light Industry, Zhengzhou, China, in 2003 and 2007, respectively, and the Ph.D. degree in power electronics and electrical drives from Shanghai Jiao Tong University, Shanghai, China, in 2012.

He is currently a Professor with the Zhengzhou University of Light Industry, Zhengzhou, China. He was a Visiting Professor with the Department of Electrical Engineering and Computer Science, The University of Tennessee, Knoxville, Tennessee, USA. He has published more than 50 technical articles in journals and conference proceedings, two books, and hold 12 Chinese patents. His research interests include model predictive control method for power converter, fault diagnosis and tolerant control of power electronics systems, and wireless power transfer. He was a recipient of the 2018 Highlighted Paper Award from IEEE TPEL.

FALONG LU received the Ph.D. degree in electrical engineering from Southwest Jiaotong University, Chengdu, China, in 2019.

He is currently a Lecturer with the Zhengzhou University of Light Industry, Zhengzhou, China. His research interests include superconducting magnetic energy storage, pulsed power supply, and electro-magnetic launch technology.